Research Article | Vol. 7, No. 8 | 1 Aug 2017 | OPTICAL MATERIALS EXPRESS 2824

Optical Materials EXPRESS

Light scattering in poly(vinyl alcohol) hydrogels reinforced with nanocellulose for ophthalmic use

GOPI KRISHNA TUMMALA,[1] NADJA FELDE,[2] SIMON GUSTAFSSON,[1] ADRIAN BUBHOLZ,[2] SVEN SCHRÖDER,[2,3] AND ALBERT MIHRANYAN[1,4]

[1]*Nanotechnology and Functional Materials, Department of Engineering Sciences, Box 534 Uppsala University, 75121 Uppsala, Sweden*
[2]*Fraunhofer Institute for Applied Optics and Precision Engineering, Albert-Einstein-Str. 7, 07745 Jena, Germany*
[3]*sven.schroeder@iof.fraunhofer.de*
[4]*albert.mihranyan@angstrom.uu.se*

Abstract: Scattering of ophthalmic devices is a complex phenomenon involving both surface and bulk light-material interactions. In this work, light scattering of nanocellulose reinforced PVA hydrogels contact lenses for ophthalmic applications was investigated. Optical microscopy, fluorescence microscopy and atomic force microscopy (AFM) techniques were used for ultrastructure characterization. Further, 3D angle resolved light scattering measurements in the visible spectral range were performed using a BTDF (bidirectional transmittance distribution function) sensor to quantify the scattered light. Surface and bulk scattering properties were discerned using white light interferometry. Total scatter levels ranging from 3% to 40% were observed depending on the hydrogel composition. The most critical factor affecting the light scattering properties in nanocellulose-reinforced PVA hydrogels was related to the state of hydration of the hydrogels, which is critical to maintain visual acuity of ophthalmic devices.

OCIS codes: (170.0170) Medical optics and biotechnology; (240.0240) Optics at surfaces; (290.0290) Scattering.

References and links

1. P. C. Nicolson and J. Vogt, "Soft contact lens polymers: an evolution," Biomaterials **22**(24), 3273–3283 (2001).
2. L. Werner and N. Mamalis, "Foldable intraocular lenses," in *Cataract and Refractive Surgery* (Springer, 2005), pp. 63–84.
3. S.-Y. Kim, Y. Honda, N. Nao-i, E. Sakaue, and M. Nambu, "A new polyvinyl alcohol hydrogel as a scleral buckling material," Am. J. Ophthalmol. **100**(2), 328–330 (1985).
4. A. M. Oelker and M. W. Grinstaff, "Ophthalmic adhesives: a materials chemistry perspective," J. Mater. Chem. **18**(22), 2521–2536 (2008).
5. K. E. Swindle and N. Ravi, "Recent advances in polymeric vitreous substitutes," Expert Rev. Ophthalmol. **2**(2), 255–265 (2007).
6. M. Zignani, C. Tabatabay, and R. Gurny, "Topical semi-solid drug delivery: kinetics and tolerance of ophthalmic hydrogels," Adv. Drug Deliv. Rev. **16**(1), 51–60 (1995).
7. N. M. Farandos, A. K. Yetisen, M. J. Monteiro, C. R. Lowe, and S. H. Yun, "Contact lens sensors in ocular diagnostics," Adv. Healthc. Mater. **4**(6), 792–810 (2015).
8. J. M. González-Méijome, M. Lira, A. López-Alemany, J. B. Almeida, M. A. Parafita, and M. F. Refojo, "Refractive index and equilibrium water content of conventional and silicone hydrogel contact lenses," Ophthalmic Physiol. Opt. **26**(1), 57–64 (2006).
9. M. G. Harris and M. D. Chamberlain, "Light transmission of hydrogel contact lenses," Am. J. Optom. Physiol. Opt. **55**(2), 93–96 (1978).
10. J. Nichols and H. Chandler, "UV protection with contact lenses," Optometry Today **51**, 8–37 (2011).
11. Ş. Ţălu and S. Stach, "Multifractal characterization of unworn hydrogel contact lens surfaces," Polym. Eng. Sci. **54**(5), 1066–1080 (2014).
12. E. Allyson and M. William, " Light scattering comparison between soft disposable contact lens wearers and non-contact lens wearers.," in *Annual Meeting of American Academy of Optometry* (Optometry and vision science, 1996).

#295836 https://doi.org/10.1364/OME.7.002824
Journal © 2017 Received 11 May 2017; revised 3 Jul 2017; accepted 5 Jul 2017; published 11 Jul 2017

Optical Materials EXPRESS

13. M. J. Giraldez and E. Yebra-Pimentel, "Hydrogel contact lenses surface roughness and bacterial adhesion," in *Ocular Diseases* (INTECH Open Access Publisher, 2012).
14. M. Katsikogianni and Y. F. Missirlis, "Concise review of mechanisms of bacterial adhesion to biomaterials and of techniques used in estimating bacteria-material interactions," Eur. Cell. Mater. **8**, 37–57 (2004).
15. T. Tanaka, M. Shigeta, N. Yamakawa, and M. Usui, "Cell adhesion to acrylic intraocular lens associated with lens surface properties," J. Cataract Refract. Surg. **31**(8), 1648–1651 (2005).
16. N. Yamakawa, T. Tanaka, M. Shigeta, M. Hamano, and M. Usui, "Surface roughness of intraocular lenses and inflammatory cell adhesion to lens surfaces," J. Cataract Refract. Surg. **29**(2), 367–370 (2003).
17. G. Rieger, "The importance of the precorneal tear film for the quality of optical imaging," Br. J. Ophthalmol. **76**(3), 157–158 (1992).
18. W. H. Ridder 3rd, A. Tomlinson, J.-F. Huang, and J. Li, "Impaired visual performance in patients with dry eye," Ocul. Surf. **9**(1), 42–55 (2011).
19. C. G. Begley, R. L. Chalmers, L. Abetz, K. Venkataraman, P. Mertzanis, B. A. Caffery, C. Snyder, T. Edrington, D. Nelson, and T. Simpson, "The relationship between habitual patient-reported symptoms and clinical signs among patients with dry eye of varying severity," Invest. Ophthalmol. Vis. Sci. **44**(11), 4753–4761 (2003).
20. R. Montés-Micó, A. Cerviño, T. Ferrer-Blasco, S. García-Lázaro, and D. Madrid-Costa, "The tear film and the optical quality of the eye," Ocul. Surf. **8**(4), 185–192 (2010).
21. B. Miljanović, R. Dana, D. A. Sullivan, and D. A. Schaumberg, "Impact of dry eye syndrome on vision-related quality of life," Am. J. Ophthalmol. **143**(3), 409–415 (2007).
22. L. C. Thai, A. Tomlinson, and W. H. Ridder III, "Contact lens drying and visual performance: the vision cycle with contact lenses," Optom. Vis. Sci. **79**(6), 381–388 (2002).
23. C. P. Lohmann, F. Fitzke, D. O'Brart, M. K. Muir, G. Timberlake, and J. Marshall, "Corneal light scattering and visual performance in myopic individuals with spectacles, contact lenses, or excimer laser photorefractive keratectomy," Am. J. Ophthalmol. **115**(4), 444–453 (1993).
24. G. T. Timberlake, M. G. Doane, and J. H. Bertera, "Short-term, low-contrast visual acuity reduction associated with in vivo contact lens drying," Optom. Vis. Sci. **69**(10), 755–760 (1992).
25. A. M. Pons, A. Lorente, C. Albarrán, R. Montés, and J. M. Artigas, "Characterization of the visual performance with soft daily wear disposable contact lenses," Ophthalmic Physiol. Opt. **18**(1), 40–48 (1998).
26. G. K. Tummala, T. Joffre, V. R. Lopes, A. Liszka, O. Buznyk, N. Ferraz, C. Persson, M. Griffith, and A. Mihranyan, "Hyperelastic Nanocellulose-Reinforced Hydrogel of High Water Content for Ophthalmic Applications," ACS Biomaterials Science & Engineering **2**(11), 2072–2079 (2016).
27. G. K. Tummala, R. Rojas, and A. Mihranyan, "Poly(vinyl alcohol) Hydrogels Reinforced with Nanocellulose for Ophthalmic Applications: General Characteristics and Optical Properties," J. Phys. Chem. B **120**(51), 13094–13101 (2016).
28. M. J. Giraldez, C. García-Resúa, M. Lira, M. E. Real Oliveira, and E. Yebra-Pimentel, "White light interferometry to characterize the hydrogel contact lens surface," Ophthalmic Physiol. Opt. **30**(3), 289–297 (2010).
29. I. G. Cox and R. H. Lee, "Understanding Lens Shape Dynamics During Off-Eye Dehydration of Contact Lens Materials with Varying Water Content," Invest. Ophthalmol. Vis. Sci. **53**, 6104 (2012).
30. . S. Schröder, M. Kamprath, A. Duparré, A. Tünnermann, B. Kühn, and U. Klett, "Bulk scattering properties of synthetic fused silica at 193 nm," Opt. Express **14**(22), 10537–10549 (2006).
31. A. Mihranyan, "Viscoelastic properties of cross-linked polyvinyl alcohol and surface-oxidized cellulose whisker hydrogels," Cellulose **20**(3), 1369–1376 (2013).
32. T. Abitbol, A. Palermo, J. M. Moran-Mirabal, and E. D. Cranston, "Fluorescent labeling and characterization of cellulose nanocrystals with varying charge contents," Biomacromolecules **14**(9), 3278–3284 (2013).
33. A. Duparré, J. Ferre-Borrull, S. Gliech, G. Notni, J. Steinert, and J. M. Bennett, "Surface characterization techniques for determining the root-mean-square roughness and power spectral densities of optical components," Appl. Opt. **41**(1), 154–171 (2002).
34. S. Schröder, A. von Finck, and A. Duparré, "Standardization of light scattering measurements," Adv. Opt. Technol. **4**, 361–375 (2015).
35. J. C. Stover, *Optical Scattering: Measurement and Analysis* Third Edition ed. (SPIE, 2012).
36. S. Schröder, M. Trost, T. Herffurth, A. von Finck, and A. Duparré, "Light scattering of interference coatings from the IR to the EUV spectral regions," Adv. Opt. Technol. **3**, 113–120 (2014).
37. S. Schröder, A. Duparré, T. Herffurth, and G. Notni, "Device and method for angularly resolved scattered light measurement," WO 002010127872 (2010).

1. Introduction

Thanks to their softness and biocompatibility, hydrogels are common ophthalmic materials that are used to treat various eye related conditions. Hydrogels are applied as soft contact lenses for vision correction purposes [1], intraocular lenses [2], scleral buckles [3], ocular wound healing adhesives [4], vitreous body replacements [5], drug delivery vehicles [6] and even as wearable diagnostic ocular devices with integrated photonic or electronic sensors [7]. In this article, hydrogel-based contact lenses will be the main focus of studies.

Optical Materials EXPRESS

In order to be used on the eye, hydrogel-based contact lenses should possess a set of optical properties. Transparency and refractive index are two important optical parameters [8, 9]. Additionally, UV-blocking properties of contact lenses are desirable to minimize the risk of cataract or pterygium [10]. Moreover, contact lens surface roughness is another important parameter affecting the optical properties of the lens [11]. Excessive surface roughness increases light scattering and thereby reduces visual acuity and, consequently, causes discomfort. Furthermore, surface roughness promotes contact lens spoilage, i.e. formation of deposits [12], as well as favors bacterial adhesion [13, 14]. Increased surface roughness may also cause inflammation as it promotes cell adhesion and release of pro-inflammatory cytokines, as previously described in intraocular lenses [15, 16].

While all engineered surfaces possess some degree of roughness, the net effect of surface roughness on optical properties is significantly affected by the presence of a water layer or, under physiological conditions, by the tear fluid film. The tear fluid film on the anterior side of the eye is the first refractive optical layer and plays a crucial role in maintaining the physiological function of the eye [17]. It is known from clinical practice that patients with dry eye disease (DED) suffer from visual malfunction manifested as blurred vision and glair as well as reduced contrast sensitivity [18, 19]. The blurred vision of DED patients is caused by an irregular tear film thickness, and the produced irregular surface roughness causes increased light scattering and, thus, visual aberrations [20]. Contrast sensitivity also decreases after tear film breakup and can cause problems in performing everyday and work-related activities, particularly in bright sunlight or at night [21]. Reduced visual acuity and contrast sensitivity have also been observed among contact lens wearers [22]. It was suggested that variations in visual performance using soft contact lenses is due to light scattering produced by the changes in the hydration levels of the lens or changes in the quality of the tear film [23, 24]. This mechanism is further supported by the notion that artificial tears can significantly improve vision both in dry eye patients not wearing contact lenses [17] and in prolonged contact lens wearers [25].

It infers from above that the surface roughness, wettability, and the state of lens hydration are critical for fulfilling its optical function. Therefore, it is important to design hydrogels with high water content without compromising the mechanical properties of the contact lens. The crux of the problem is that normally excessive water content implies poor mechanical properties, while reinforcement of the hydrogel with stiff additives negatively impacts the optical performance, e.g. transparency and light scattering.

In this context, we have recently described how the dilemma between hydrogel softness and strength of contact lenses at high water content can be resolved, while maintaining the desirable optical transparency [26]. In particular, we developed highly transparent hydrogels composed of soft Poly(vinyl alcohol) (PVA) polymer matrix reinforced with relatively stiff cellulose nano crystals (CNC) / cellulose nanofibers (CNF). The produced hybrid hydrogels feature exceptionally high water content, i.e. 90-93 wt%, and exhibit hyperelastic mechanical properties similar to that of natural tissue, i.e. collagen [27]. Furthermore, these hybrid hydrogel lenses demonstrate a set of remarkable optical properties such as refractive index close to that of water, i.e. 1.33, high transparency in the visual range, i.e. > 95%, and mild UV-blocking properties, i.e. 40-50% [27]. Furthermore the material shows good cytocompatibility with corneal epithelial cells both in direct and indirect (leachables) cell tests [26].

In this paper, the light scattering properties of these hybrid PVA-nanocellulose hydrogels are analyzed. Angle resolved scattering measurements in the visible spectral range are performed to quantify the scattering distribution and scatter losses. Utilizing a specific scatter sensor enables scatter measurements to be performed within a few seconds and thus samples to be studied in different drying states. In combination with surface metrology data a differentiation in relation to bulk and surface effects is made.

Optical Materials EXPRESS

2. Results and discussion

Reduced visual performance of the reinforced PVA hydrogels can be expected to be caused by light scattering from both the hydrogel surface and from the bulk material itself. In order to separate these effects and to assess the impact of surface scattering, surface roughness investigations are necessary. In that respect atomic force microscopy (AFM) and white light interferometry (WLI) are two of the most common techniques to study surface roughness of contact lenses [28]. Utilizing the morphology data can provide a distinction in roughness and bulk induced light scattering as presented in the following.

2.1 Analysis of microscopy

Three different microscopy techniques were used to investigate and understand the internal structure of hydrogels in their native wet state. In particular, the distribution of nanocellulose in the hydrogel matrix is a fundamental question of interest to understand the light scattering in hydrogels of different composition and thickness. Figures 1(a)-1(c) show the optical microscopy images of the hydrogels. The hydrogels present an open macro-porous honeycomb like structures with pore openings extending up to few tens of micrometers. The pore size was slightly different among hydrogels of different composition owing to nano-structural interactions between the PVA matrix and nanocellulose moieties. The dark patches causing light occlusion in PVA-CNF hydrogel are probably due to CNF aggregates present in the lower planes than the plane of imaging. The formation of CNF aggregates is due its high viscosity related to high aspect ratio of CNF.

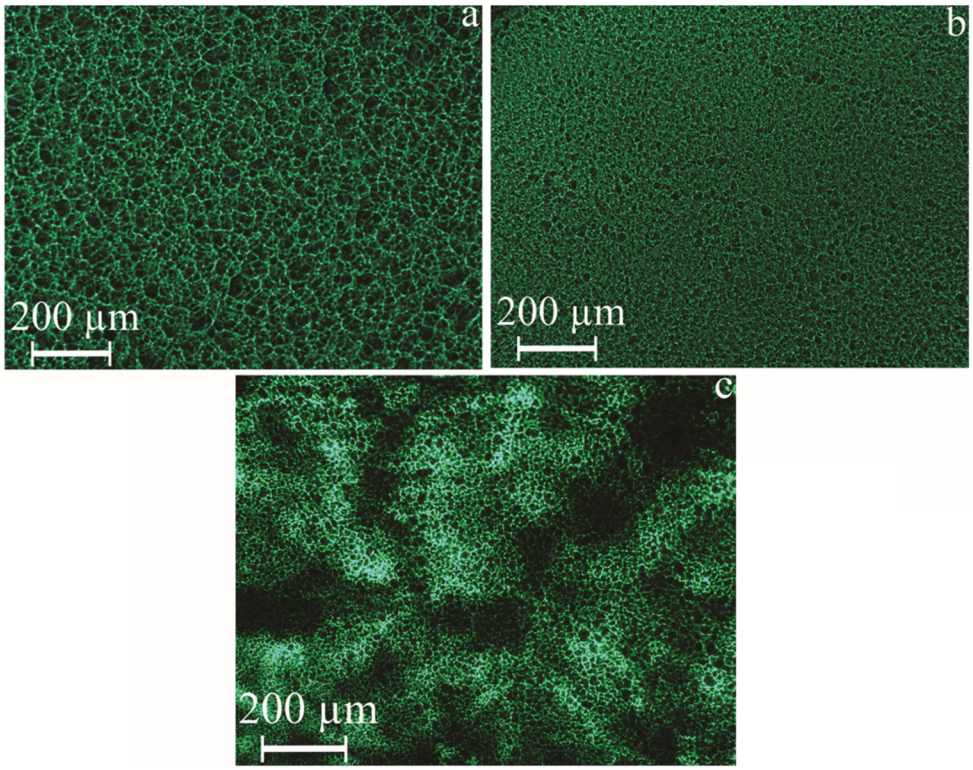

Fig. 1. Optical light micrographs of (a) pure PVA, (b) PVA-CNC and (c) PVA-CNF hydrogels.

Figures 2(a)–2(c) show the fluorescence microscopy images of hydrogels where nanocellulose components were labelled with fluorophore groups, i.e. DTAF 5-(4, 6-dichlorotriazinyl) amino fluorescei. While it is not expected that fluorescence imaging could

Optical Materials EXPRESS

provide information about individual nanocellulose units due to low resolution of the technique, it still provided some clues about the distribution of nanocellulose inside the hydrogel. It can be seen that CNC are distributed much more homogeneously than CNF, which tend to form lumps. As expected, the control pure PVA hydrogel showed negligible fluorescence, and the tiny fluorescent spots may be attributed to residual double bond chemical structures in PVA.

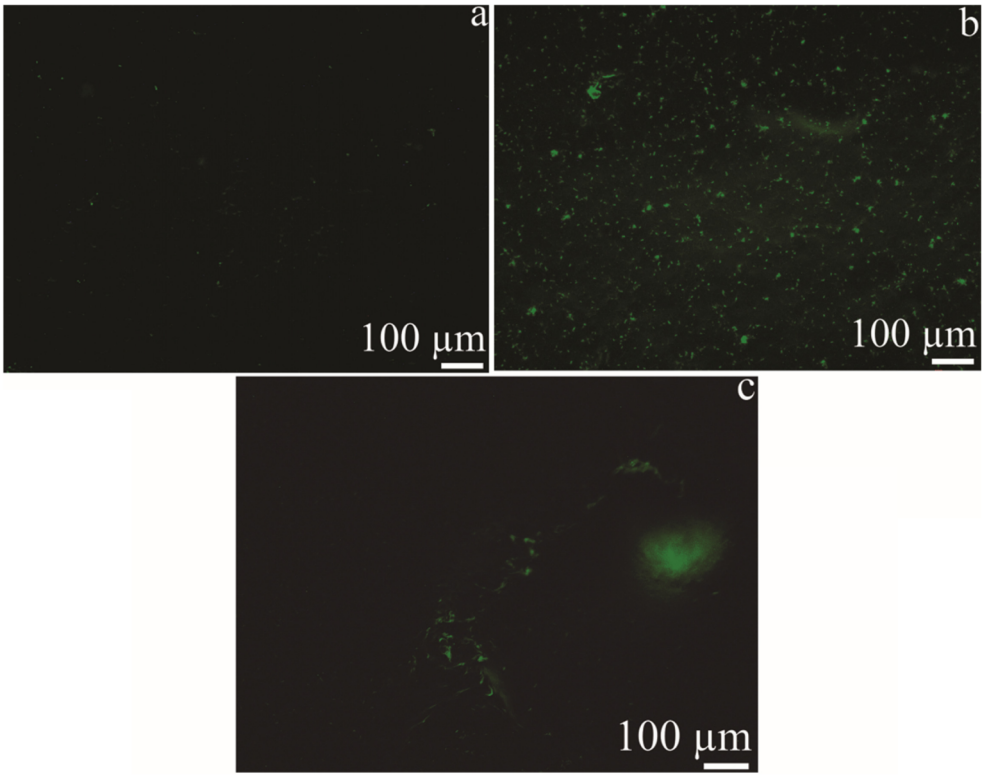

Fig. 2. Fluorescent micrographs of (a) pure PVA, (b) PVA-CNC and (c) PVA-CNF hydrogels.

Figures 3(a)–3(c) show the AFM micrographs of the hydrogels in wet state, i.e. immersed in water. The surface topography of pure PVA sample exhibits a wavy pattern of moderate ruggedness. The surface topography of PVA-CNC sample appears rougher, as compared to pure PVA samples, and featured with sharp spikes. The distribution of these sharp spikes in Fig. 3(b) is comparable to the distribution of fluorescently labeled CNCs in Fig. 2(b). In PVA-CNF samples the surface topography is also rougher, compared to pure PVA sample, with clearly visible relatively sharp peaks.

Optical Materials EXPRESS

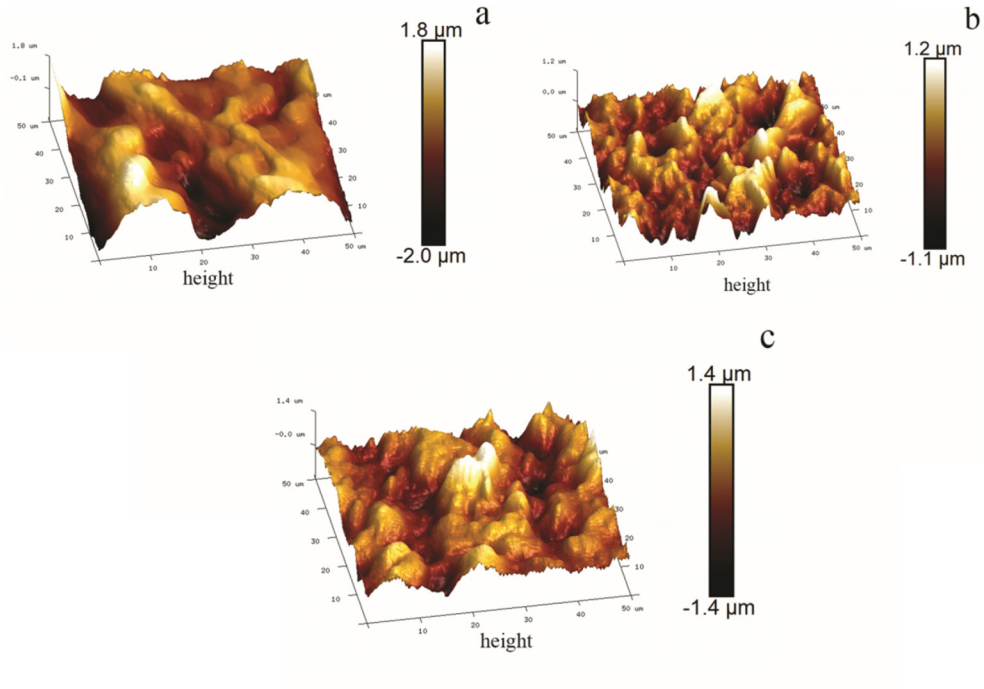

Fig. 3. AFM topography images of (a) pure PVA, (b) PVA-CNC and (c) PVA-CNF hydrogels.

2.2 Analysis of light scattering properties

To evaluate the optical properties close to the real application conditions, measurements in the wet state are essential. However, a major obstacle is the fast drying of the samples after removal from the immersion liquid. Consequently, there is only a small time window of some seconds to estimate the light scattering properties of the hydrogels under real application conditions. It should be noted that rapid (within minutes) drying and shrinking of hydrogel-based contact lenses is normal and was previously described in the literature (under physiological conditions the tear fluid film layer evaporation from the eye is prevented through blinking) [29].

The above-mentioned drastic change of the scattering properties as a function of the hydration state of the samples is illustrated in Fig. 4. The illustration in Fig. 4(a) shows the 3D angle resolved scattering (ARS) measurements with the total scattering (TS) levels as well as the WLI topography images of the thin PVA-CNC sample at different time intervals after removal from the immersion liquid. For detailed analysis of the scattering the azimuthal averaging of data was performed to obtain the 1D ARS, also depicted in Fig. 4(b). A significant change of ARS is already observable after 10 min in air, especially at small scattering angles. The ARS data at angles >10° remains almost constant, indicating a pronounced surface effect. The WLI measurements confirm this statement.

Optical Materials EXPRESS

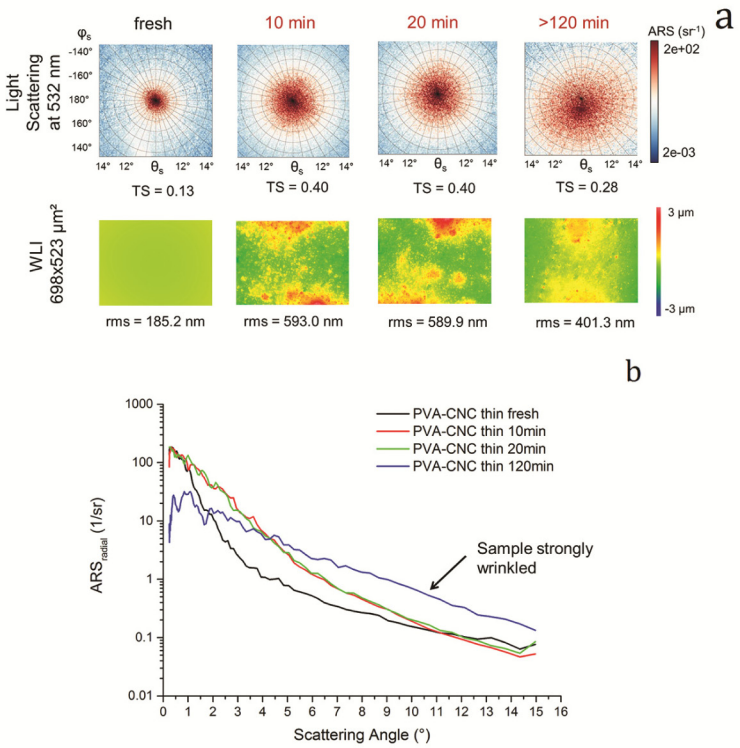

Fig. 4. (a) 3D ARS and WLI measurements and (b) 1D ARS for thin PVA-CNC sample at different drying states.

In the state immediately after removing the sample from the immersion liquid, the liquid in the bulk of the sample as well as the liquid film on the surface lead to a smoother index transition from the PVA surface to the water causing less light scattering (TS = 0.13). With increasing drying time the surface roughness revealed, which results in higher surface light scattering (TS = 0.4). Already after 10 min in air, the thin sample becomes rigid. Consequently no further change in surface roughness or scattering with increased drying time is observed until the sample loses its form and becomes strongly wrinkled, which complicates the measurement procedure. WLI analysis of thick samples showed negligible differences in surface roughness compared to the thin samples.

Thus, in order to discern bulk and surface scattering properties of the hydrogels, quick measurements with the Bidirectional Transmittance Distribution Function (BTDF) sensor, performed directly after removing the hydrogel samples from water, were found to be essential.

The results of these scattering measurements demonstrate significant variations between the ARS data of the different materials pure PVA, PVA-CNC and PVA-CNF. Regarding the thick samples (5 mm thickness) reduced light scattering was observed for pure PVA. The PVA samples with CNF evince the highest scattering level, which is about one order of magnitude higher in comparison to PVA-CNC and pure PVA (see Fig. 5). The presumable cause of this behavior is inhomogeneous distribution of CNF in the hydrogel as discussed above.

Optical Materials EXPRESS

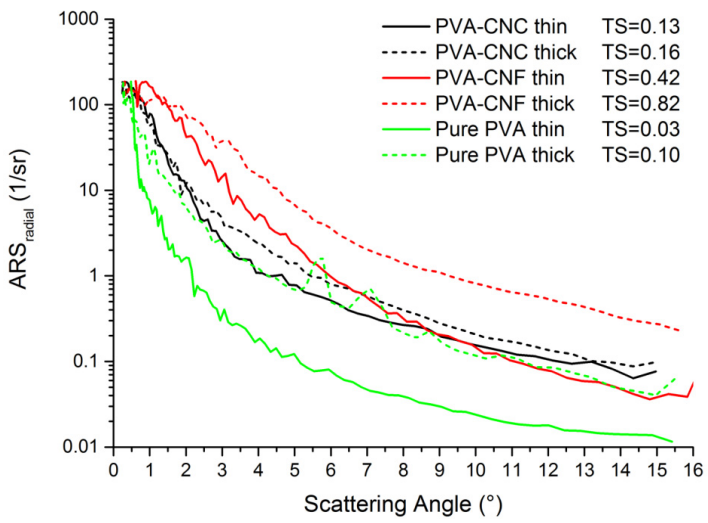

Fig. 5. 1D ARS data by azimuthal averaging of the 3D ARS data for pure PVA, PVA-CNC and PVA-CNF samples.

These optical properties can be related to the bulk material as the roughness analysis of the wet and dry hydrogel surfaces showed negligible differences between the investigated material surfaces in the light scattering relevant spatial frequency range (see Fig. 6).

However, analyzing the results of the scattering measurements for different thick samples allows a more detailed differentiation in relation to bulk and surface effects. The scattering data of the 0.3 mm thin samples compared to the scattering properties of the 5 mm thick samples are shown in Fig. 7. The TS levels calculated from the ARS data are also provided. The ARS levels as well as the scattering losses are obviously reduced for the thinner samples of 0.3 mm for PVA-CNC, PVA-CNF and for pure PVA. Assuming that the influence of surface scattering is similar for thin and thick samples, higher total scatter indicates a significant amount of bulk scattering caused by inhomogeneities in the thick hydrogels.

Optical Materials EXPRESS

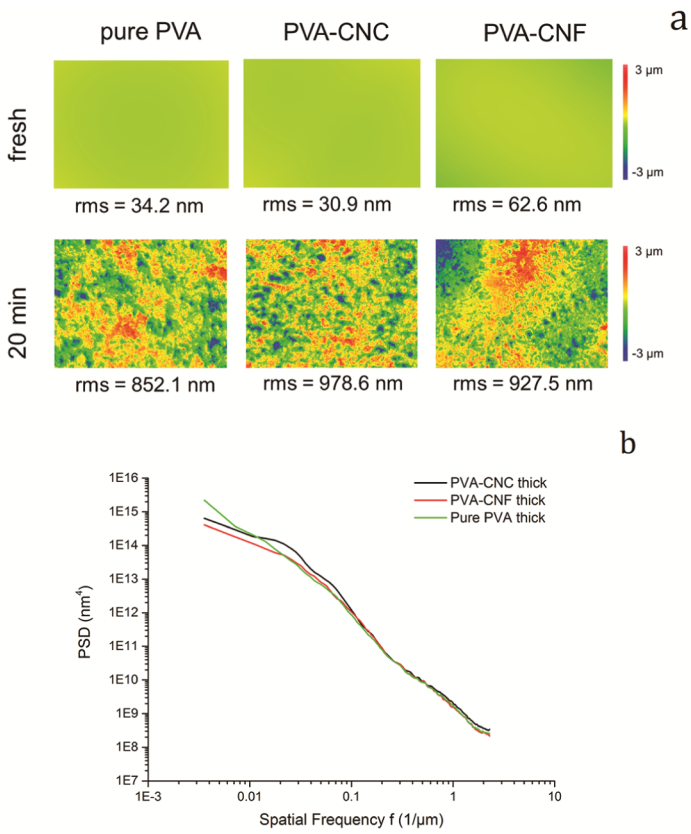

Fig. 6. (a) WLI images (698x523 µm^2) of thick hydrogels in wet condition and after 20 min drying time (surface smoothing by liquid film in wet condition) and (b) power spectral density (PSD) functions after 20 min drying time.

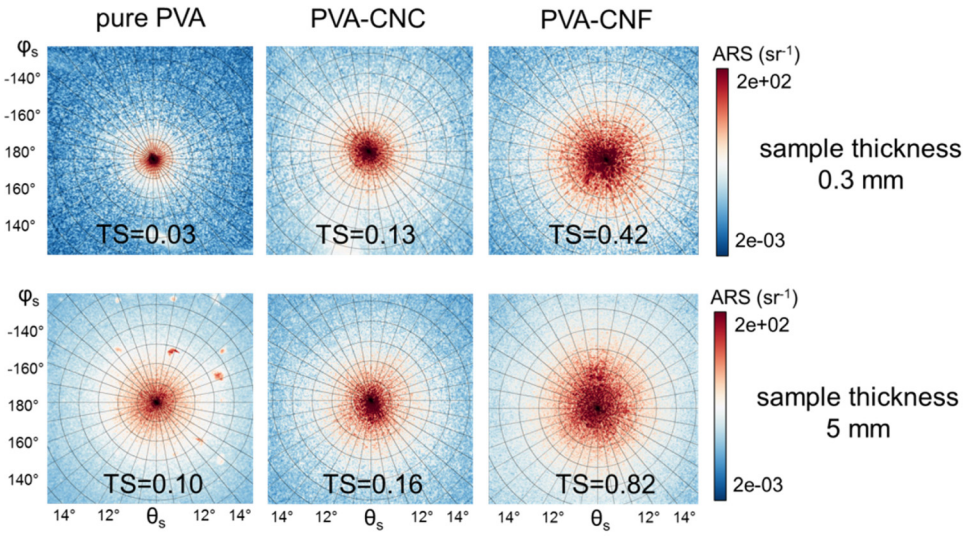

Fig. 7. 3D ARS data and TS levels for pure PVA, PVA-CNC and PVA-CNF (upper row: thin samples of 0.3 mm; lower row: thick samples of 5 mm).

Optical Materials EXPRESS

A detailed depiction was already shown in Fig. 5 using the 1D ARS data. The smallest difference in scattering between the thick and thin samples was observed for the PVA-CNC sample, even though the sample includes cellulose nanocrystals in its bulk as opposed to pure PVA. The increased scattering for pure PVA could be a result of larger pore size and thicker pore walls as visualized in the optical microscopy images (see Fig. 1). It should be noted that PVA-CNF sample provoked higher scattering levels in the bulk material in comparison to both pure PVA and PVA-CNC. Primarily this behavior is assumed to result from CNF aggregates in the bulk material as indicated in the microscopy data.

Finally, as a quantitative statement, the bulk scattering coefficient α can be estimated from the measured data, as shown in Fig. 8. Since the roughness of the thin and the thick samples is almost identical, the roughness-induced contribution to the observed scattering is the same for both samples. The observation that the total scattering is increasing with sample thickness can thus be entirely attributed to bulk scattering caused by inhomogeneities in the materials, as discussed above. The total scattering can therefore be assumed to be directly proportional to sample thickness, even though more data points would have been better to prove this claim as showed in our previous work [30]. Roughness-induced surface scatter only leads to a constant offset of the data independent of the sample thickness. Following this argumentation, the bulk scattering coefficient is simply the slope of the curve. As can be seen from the graph, the highest bulk scattering coefficient, i.e. $\alpha = 0.85\ cm^{-1}$, was observed for PVA-CNF sample. This is in agreement with the microscopy data revealing a rather inhomogeneous distribution of CNF aggregations within the material.

In all, the results of the present study highlight the importance of intact water film layer on the surface of hydrogel samples to minimize light scattering similar to what is normally observed under the physiological conditions on the eye.

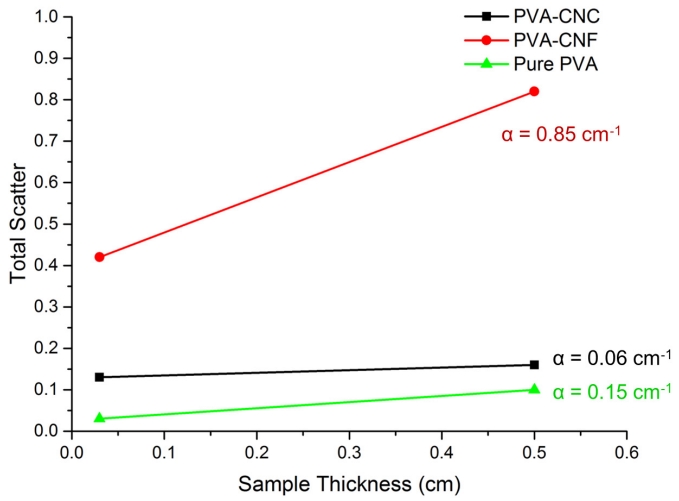

Fig. 8. Estimation of bulk scattering coefficients for pure PVA, PVA-CNC and PVA-CNF samples.

3. Conclusion

The results of the present study suggest that nanocellulose reinforced PVA hydrogels for ophthalmic use possess low light scattering properties when fully wetted, especially in PVA-CNC sample. The drying of the samples depletes the surface water film and increases the surface roughness, which inevitably increases the level of surface light scattering. In wet condition, however, bulk scattering is the main light scattering source. The bulk light

Optical Materials EXPRESS

scattering was more pronounced in the thick samples as expected. Especially high was the scattering in PVA-CNF hydrogel, which is believed to arise due to CNF aggregation and inhomogenous distribution. PVA-CNC hydrogels present promising candidates for further development of high water content biocompatible ocular devices.

4. Materials and methods

4.1 Materials

Microcrystalline cellulose -Avicel PH 101 (MCC), 2,2,6,6-tetramethylpiperidine-1oxyl radical (TEMPO), 4-Acetamido-TEMPO, NaBr, NaClO, $NaClO_2$, $CH_3COONa{\cdot}3H_2O$, NaOH, poly(vinyl alcohol) with Mw_{AVG} 146,000-186,000 and degree of saponification 99.9%, (PVA), dimethyl sulfoxide (DMSO), HCl, 5-(4, 6- dichlorotriazinyl) aminofluorescein (DTAF) were purchased from Sigma Aldrich. All the chemicals used were of reagent grade or better. Deionized water was used for all experiments.

4.2 TEMPO mediated oxidation of cellulose

To produce cellulose nanocrystals (CNC), MCC was oxidized according to a previously published method [31]. In short, 5 g MCC was dispersed in 400 ml of deionized water and 90 mg of TEMPO and 1 g of NaBr solubilized in 100 ml deionized water were added to it. The mixture was kept under magnetic stirring at 500 RPM. To the mixture, 10 ml of 10% wt NaClO with pH of 11 adjusted with 1M HCl was added at intervals of 30 min for 3.5 hours (70 ml in total). The reaction system was maintained at pH 10.5 by adding 1 M NaOH through the entire period of reaction. The reaction was quenched after 3.5 hours by adding 10 ml of ethanol. Oxidized MCC was washed 3 times with deionized water by centrifugation and then dialyzed for 3 days. Cellulose was then collected by centrifuging and was dispersed in deionized water by ultrasonication (Vibracell 700 W, 20 KHz, USA) for 5 min to obtain a transparent gel.

Cellulose nanofibrils (CNF) were prepared from never-dried spruce sulfite pulp using 4-Acetamido-TEMPO as previously described [27]. The pulp (10 g) was suspended in 0.1 M acetate buffer (1000 ml, pH 4.8) and stirrer using an overhead stirrer at 150 RPM until fully dispersed. Thereafter, 4-Acetamido-TEMPO (1 mmol) and sodium chlorite (0.1 mol) were added until dissolution. A buffered (pH 4.5); 30 ml of a 2 M NaClO solution (10.0 mmol) was added to the reaction flask in three steps, 10 ml each/2 hours. The reaction flask was maintained under nitrogen atmosphere over a period of 48 hours at 60 °C with continuous stirring. The oxidation product was thoroughly washed, and the pulp fibers were mechanically dispersed in deionized water at 1% wt using high-shear homogenization. The final dispersion had a solid content of 0.6% wt.

4.3 Preparation of hydrogel

To produce the hydrogels, 3 g of PVA was added to a mixed solvent system of DMSO and deionized water so as to obtain a concentration of 10% (w/w). The composition of solvent was varied by changing the mass ratios of DMSO and water to obtain DMSO:water 80:20, 70:30 and 60:40 mixtures. PVA solutions were obtained by heating the mixture at 100 °C under stirring in an oil bath for about 2 hours. For the preparation of a composite hydrogel, nanocellulose (1% wt of PVA) was added to the PVA solution and further mixed for an hour at 100 °C. The homogenous and transparent solutions obtained by this method were cast in to respective molds of different sizes and shapes and allowed to gel at –20 °C for 24 hours. The thickness is controlled by the size of the molds. The formed gels were collected from the molds, and the DMSO was exchanged with deionized water by dialyzing the gels in excess water for at least 48 hours. The obtained products after washing were stored in deionized water for further testing. Utilizing this procedure 0.3 mm, 5 mm and 12.5 mm thick disc shaped samples of pure PVA, PVA-CNC and PVA-CNF were made.

Optical Materials EXPRESS

4.4 Optical microscopy

An Olympus AX70 microscope was used to acquire images of the hydrogels. For microscopy 12.5 mm thick disc shaped samples were used. The microscope was mounted with a CCD camera, and DeltaPix software program was used to take the pictures. IF 550 green contrast color filter was used for better visualization.

4.5 Fluorescence microscopy

CNC and CNF were labelled with DTAF according to a previously reported procedure [32]. Both CNC (500 mg) and CNF (500 mg) were reacted with DTAF (7.5 mg) under alkaline conditions (0.2M NaOH) for 24 h, in the dark with magnetic stirring. The mass ratio of both CNC and CNF to DTAF were kept constant (500 mg CNC/CNF: 7.5 mg DTAF), the volume of the reactions depends on initial concentration of the nanocellulose suspension. Solid NaOH and DTAF were added to CNC/CNF suspension. Volume of the reaction was adjusted appropriately to obtain a 1 wt% suspension of CNC/CNF. To remove the unreacted DTAF and NaOH, samples were washed with deionized water by centrifuging 6 times. Washed samples were dialyzed for 72 h under dark conditions by changing water every 24 h. Dialyzed samples were centrifuged to remove excess water and later sonicated for 5 minutes to homogenize the samples.

Fluorescent images of nanocellulose distributed in hydrogel lenses were obtained using Nikon eclipse TE2000-U microscope equipped with a camera. Fluorescence was measured using excitation wavelength of 494 nm and emission wavelength of 512 nm.

4.6 Atomic force microscopy

A Bruker BioScope Catalyst instrument with a Bruker PFQNM-LC-A-CAL probe was used to obtain the images in a field of 50x50 μm^2. The probe is 17 µm tall, has a 65 nm tip radius and a spring constant of 0.1 N/m which makes it suitable for measuring soft materials. All the samples were mounted in a petri dish then submerged in Milli-Q water prior during the measurement. The images were acquired in peak-force tapping mode, post processing of the images and surface roughness calculations were done in Bruker's NanoScope Analysis v 1.6 software.

4.7 White light interferometry and roughness analysis

In addition to the optical microscopy investigations of the different hydrogels, a quantitative characterization of the surface structures of the hydrogels was performed by White Light Interferometry measurements (WLI, NewView7300/ZygoLOT) using 10x and 50x objectives. This results in a range of lateral surface spatial frequencies from 0.002 μm^{-1} to 2.3 μm^{-1}, which covers the spatial frequency range relevant for light scattering at visible wavelengths. Using the WLI topographic surface data (h(x,y)) two-dimensional isotropic power spectral density (PSD) functions of every sample were calculated for roughness analysis as described in our previous work [33]. The rms-roughness σ, defined as the standard deviation of the surface heights, can be determined by integrating these PSD function over the relevant spatial frequency range:

$$\sigma^2 = 2\pi \int_{fmin}^{fmax} PSD(f) f df. \quad (1)$$

In contrast to simple roughness measurements, this PSD based procedure allows us to combine different measurements and to retrieve roughness values representative for the entire spatial frequency range relevant for visible light scattering. Moreover, the scattering distribution or Angle Resolved Scattering (ARS) is directly proportional to the surface PSD. For a single surface, which is clean and optically smooth, the Rayleigh-Rice theory predicts [34, 35]:

Optical Materials EXPRESS

$$\mathrm{ARS}(\theta_s) = Q \cdot \mathrm{PSD}(f). \quad (2)$$

The optical factor Q contains information such as the conditions of illumination and observation as well as material properties. Within this equation, the spatial frequencies and the scattering angles are related by the grating equation:

$$f = (\sin\theta_s)/\lambda. \quad (3)$$

For visible light applications, assuming λ_{min} = 380 nm and λ_{max} = 780 nm and scattering angles between 0.1° and 90°, the relevant spatial frequencies for normal incidence consequently ranges between 0.002 μm^{-1} and 2.6 μm^{-1}.

4.8 Light scattering

Angle resolved light scattering measurements were performed to investigate the optical properties of the hydrogel materials. Usually, highly sensitive goniometric scatterometers are used, which are based on scanning a detector about the illuminated sample [36]. In this study, a BTDF (Bidirectional Transmittance Distribution Function) Sensor [37], recently developed at Fraunhofer IOF, was used. In contrast to conventional scatterometers, the BTDF sensor enables scatter measurements within a few seconds and thus allows samples to be measured before drying out. In the setup (Fig. 9), a tunable supercontinuum source was used at a wavelength λ of 532 nm to illuminate the clamped hydrogel samples at an angle of incidence of θ_i = 0°. The wavelength was chosen because it lies in the most relevant part of the spectrum visible to the human eye. A CMOS detector matrix and a high dynamic range (HDR) procedure were used to measure the scattered light in the transmission hemisphere in a cone angle of 14° around the specular beam.

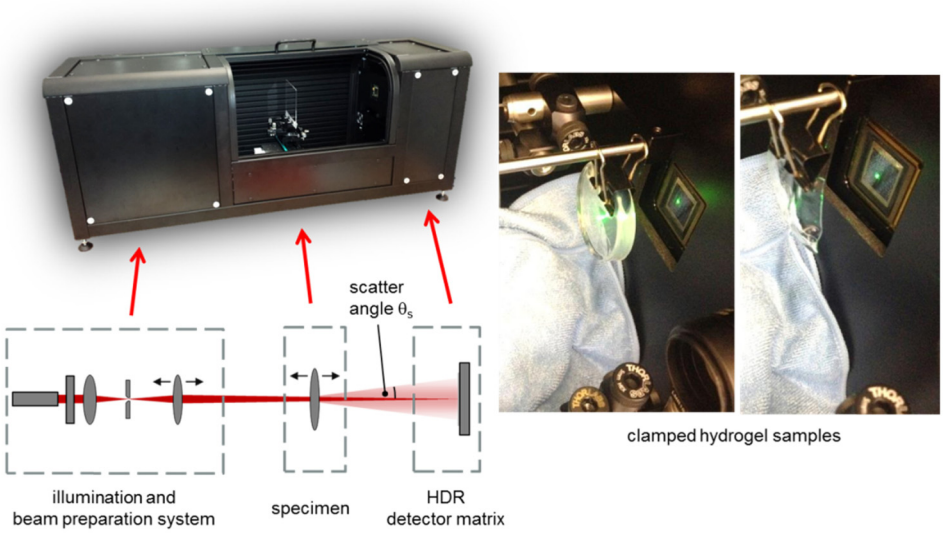

Fig. 9. Setup for light scattering measurements of hydrogel samples using the BTDF sensor.

As the instrument enables rapid 3D scattering measurements, i.e. within a few seconds, 0.3 mm and 5 mm disc shaped samples of pure PVA, PVA-CNC and PVA-CNF were investigated at different stages of drying after removal from the immersion liquid (water) including almost fully wet conditions.

The 3D scattering distributions were quantified in terms of the ARS, defined as the power ΔP_s of the light scattered into the solid angle $\Delta\Omega_s$, normalized to $\Delta\Omega_s$ and the incident light power P_i [34, 35]:

Optical Materials EXPRESS

$$\mathrm{ARS}(\theta_s) = \left(\Delta P_s(\theta_s)\right) / \left(\Delta \Omega_s P_i\right) \quad (4)$$

where θ_s is the scattering angle with respect to the surface normal. ARS is identical to the cosine corrected bidirectional transmittance distribution function, where BTDF = ARS/cos(θ_s). Additionally, total forwardscatter (TS_f) data were retrieved by integration of the ARS to compare the light scattering properties of the PVA samples. Total forwardscattering (TS_f) is defined as the total scattered power P_s in the transmission direction normalized to the incident power P_i [34, 35]. In the text, total forwardscatter (TS_f) is referred to simply TS.

Funding

Knut and Alice Wallenberg Foundation.

Acknowledgements

One of the authors (A.M.) is a Wallenberg Academy Fellow and thanks the Knut and Alice Wallenberg Foundation for their long-term financial support.